Current Biology, Volume *29*

Supplemental Information

A Retino-retinal Projection Guided by Unc5c

Emerged in Species with Retinal Waves

Verónica Murcia-Belmonte, Yaiza Coca, Celia Vegar, Santiago Negueruela, Camino de Juan Romero, Arturo José Valiño, Salvador Sala, Ronan DaSilva, Artur Kania, Víctor Borrell, Luis M. Martinez, Lynda Erskine, and Eloísa Herrera

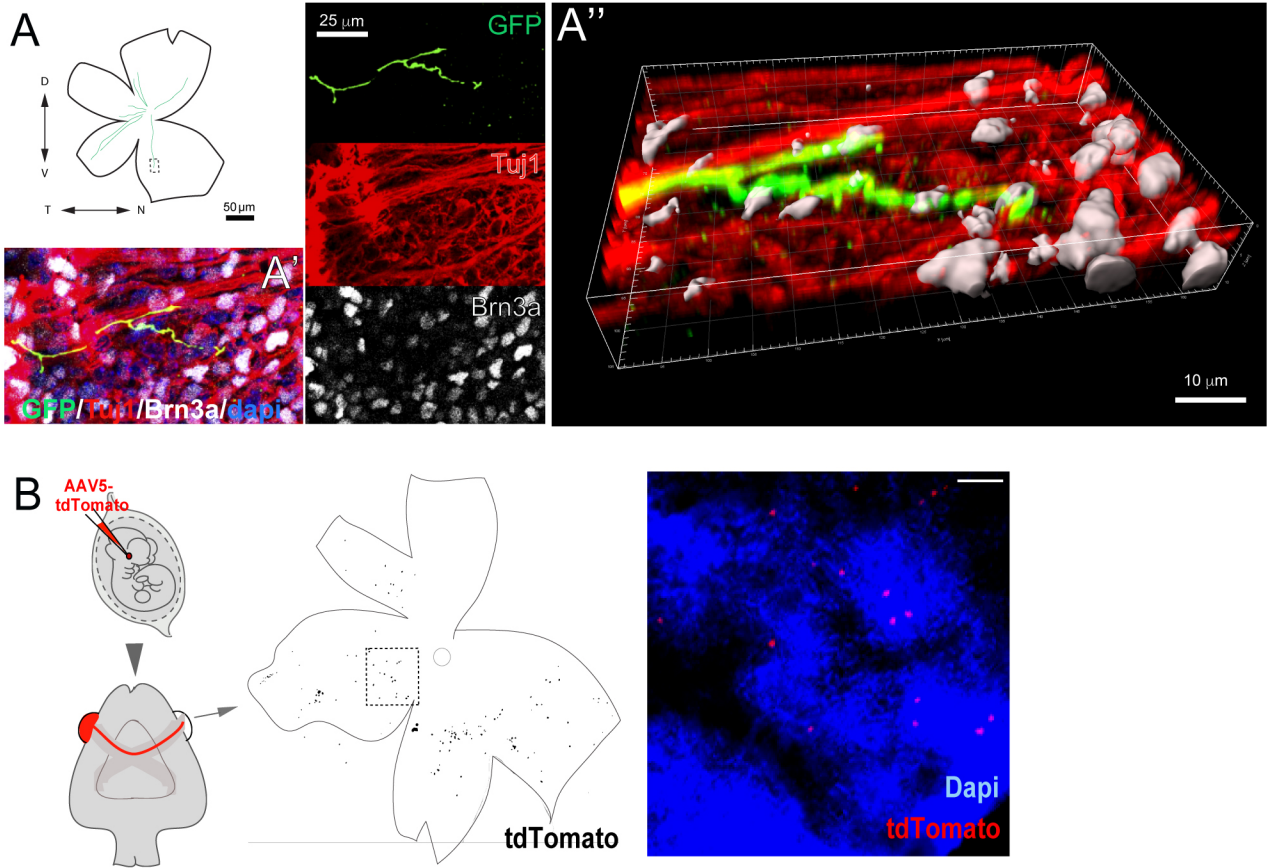
A
D
V
T
N
50 μm
25 μm
GFP
Tuj1
Brn3a
A'
GFP/Tuj1/Brn3a/dapi
A''
10 μm
B
AAV5-
tdTomato
tdTomato
Dapi
tdTomato

Figure S1. Characterization of the R-R projection. Related to Figure 1. (A) Drawing of a P2 retina containing R-R axons labeled by electroporation at E.13.5. (A') High magnification of the boxed region in (A) showing an eGFP-R-R axon terminal in a retina incubated with Tuj1 (red) and Brn3b (white) antibodies. The three channels are shown separately at the right. (A'') 3D reconstruction of a z-stack captured from the boxed area in "A". (B) Retrograde labeling by AAV5-infection. The drawing at the left summarizes the experimental procedure for retrograde viral infection. AAV5-tdTomato viruses (red) were injected into one retina of E13.5 embryos and 10 days later the contralateral retina was analyzed. The color-inverted whole-mounted retina at the right shows the distribution of RGCs retrogradely labeled from a P5 pup injected with the AAV5-tdTomato virus at E13.5. The td-Tomato cells are located predominately at the ventral part of the central retina. Image at the right, higher magnification of the boxed region.

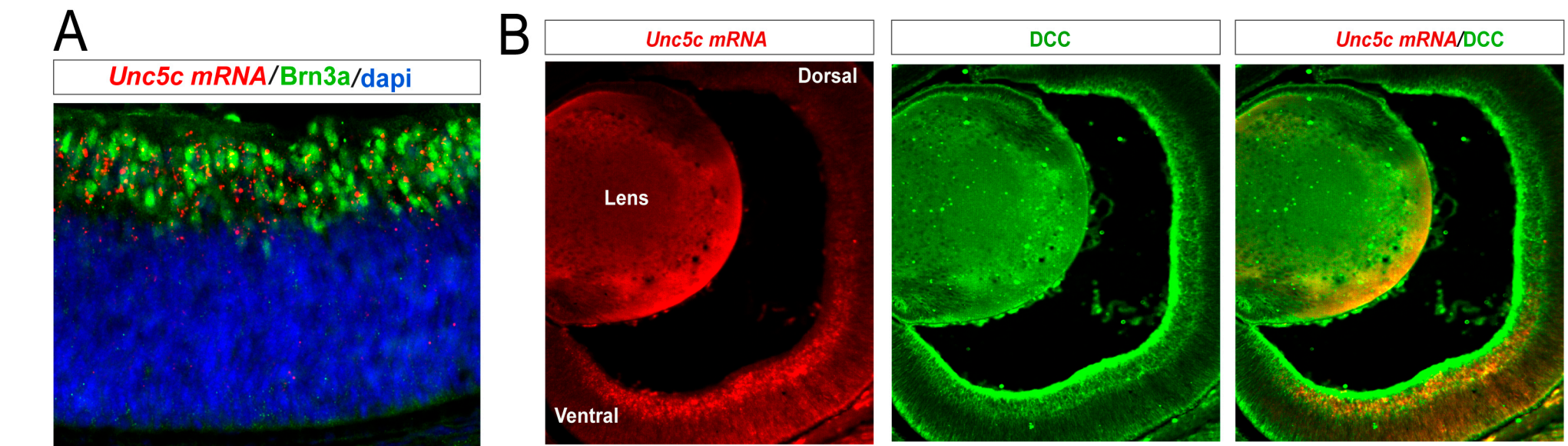
A
Unc5c mRNA/Brn3a/dapi
B
Unc5c mRNA
DCC
Unc5c mRNA/DCC
Dorsal
Lens
Ventral

Figure S2. *Unc5c* and *DCC* expression in the developing retina. Related to Figure 3.

(A) Immunohistochemistry for Brn3a (green) combined with ISH for *Unc5c* (red) in a coronal section through an E16.5 mouse retina counter stained with dapi (blue). *Unc5c* is expressed in the RGC layer.

(B) Immunostaining for Dcc (green) combined with ISH for *Unc5c* (red) in a coronal section through an E15.5 mouse retina.

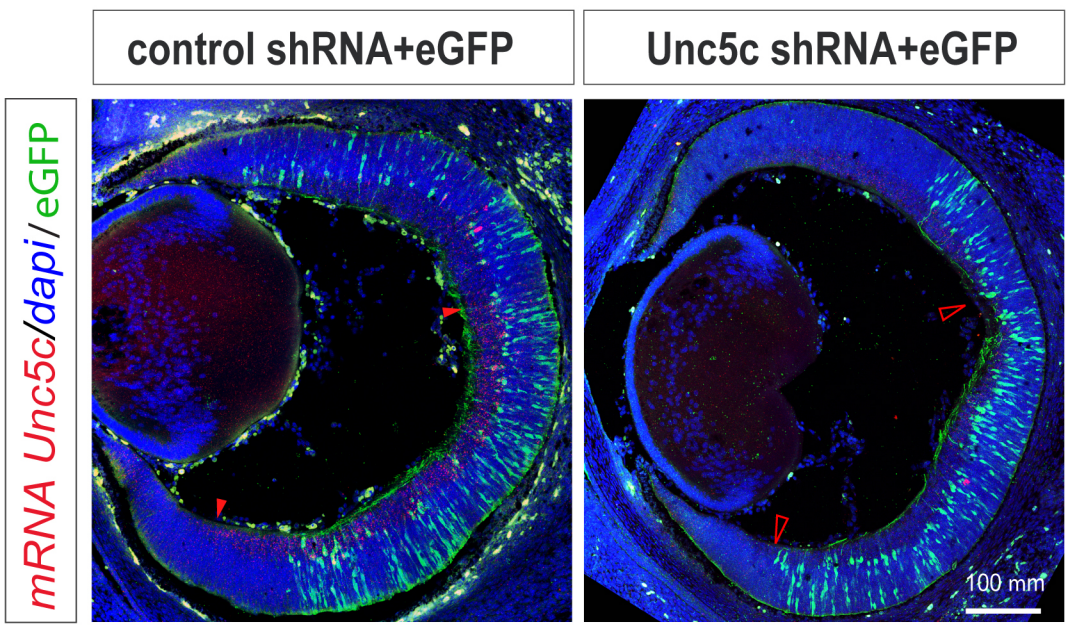
control shRNA+eGFP
Unc5c shRNA+eGFP
mRNA Unc5c/dapi/eGFP
100 mm

Figure S3. Downregulation of retinal *Unc5c* by shRNA electroporation. Related to Figure 4.

ISH for *Unc5c* (red) in coronal retinal sections from E16.5 embryos electroporated at E13.5 with control shRNA+eGFP or Unc5c shRNA+eGFP (green) and counter stained for DAPI (blue). After electroporation of Unc5c shRNA+eGFP, *Unc5c* expression (open arrowheads) is downregulated compared to the control retinas (red arrowheads).

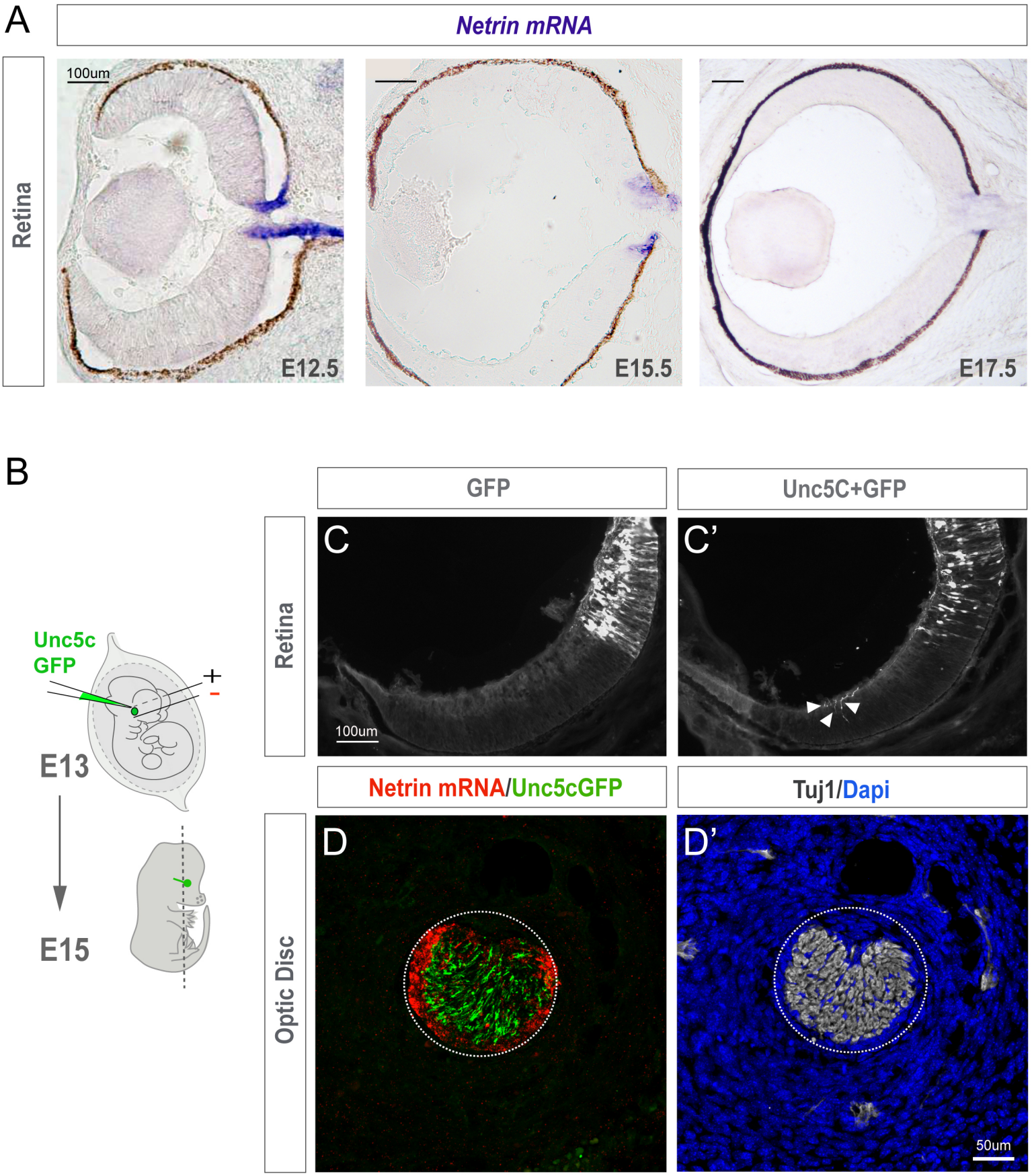
A
Netrin mRNA
Retina
100um
E12.5
E15.5
E17.5
B
GFP
Unc5C+GFP
Retina
C
C'
100um
Unc5c
GFP
+
-
E13
E15
Netrin mRNA/Unc5cGFP
Tuj1/Dapi
Optic Disc
D
D'
50um

Figure S4. *Netrin* expression and intraretinal guidance in Unc5c electroporated retinas. Related to Figure 6.

(A) ISH for *Netrin1* in coronal sections through E12.5 – E17.5 wild-type retina. At E12.5 *Netrin1* is highly expressed in the optic stalk. At later stages (E15.5-E17.5) *Netrin1* expression at the optic stalk decreases.

(B) eGFP or Unc5c/GFP encoding plasmids were electroporated into one eye of E13.5 embryos and axon trajectory analysed at E15.5.

(C-C') In control embryos, eGFP electroporated RGCs send their axons through the optic disc (C). In embryos electroporated with Unc5c/GFP some labelled RGCs misproject inside the retina, rather than exiting the eye (arrowheads, C').

(D-D') ISH for *Netrin1* in a transversal section throughout the optic disc of an E15.5 embryo electroporated at E13.5 with Unc5c/GFP encoding plasmids. (D) Despite Netrin1 expression in the optic disc, many axons expressing Unc5c/GFP are able to exit the retina growing through the Netrin1 ring surrounding the optic disc. (D') Tuj-1 and dapi stainings in the same section as (D) to visualize RGC axons exiting the retina and the anatomy of the optic disc.

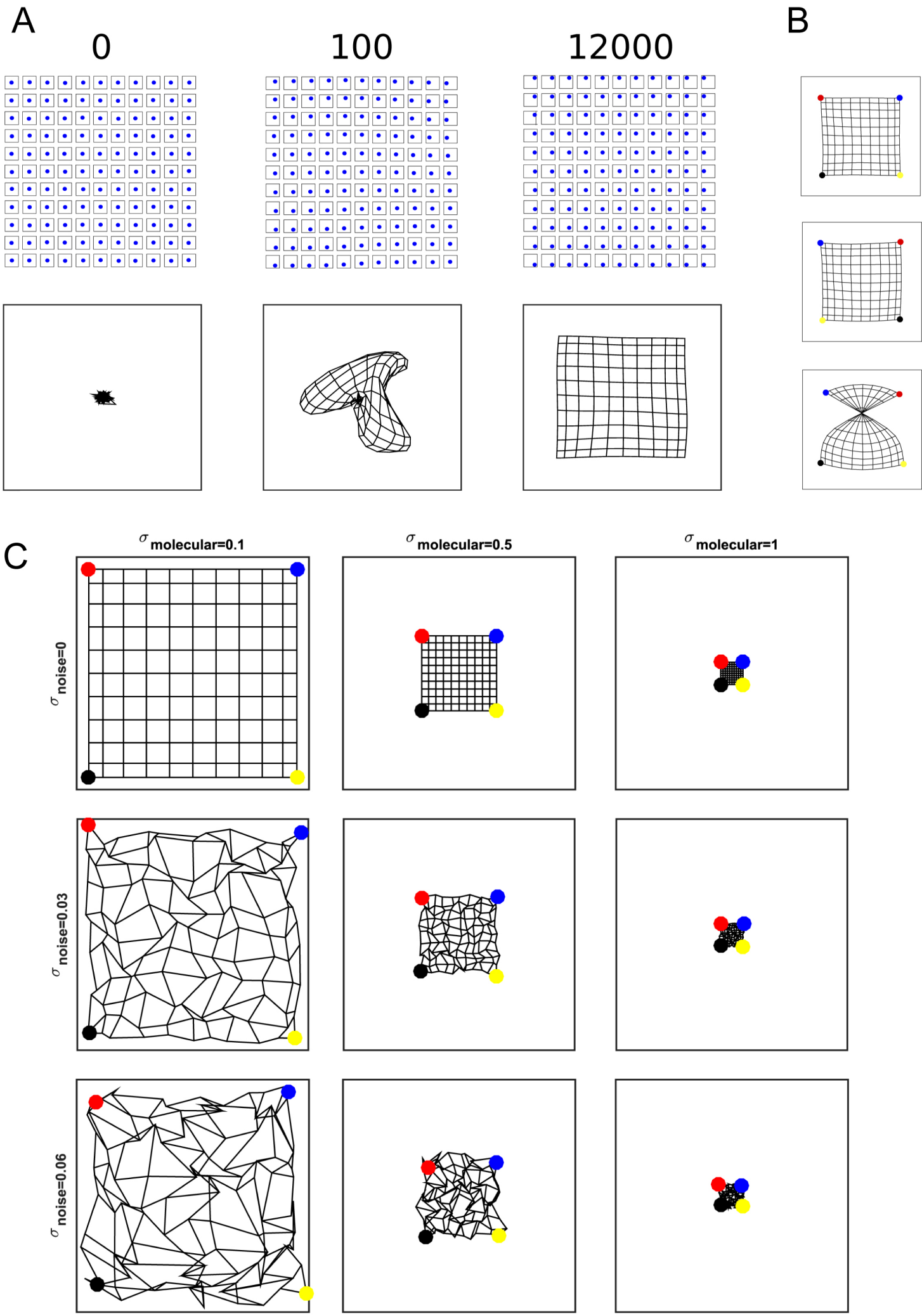
A
0
100
12000
B
C
σ molecular=0.1
σ molecular=0.5
σ molecular=1
σ noise=0
σ noise=0.03
σ noise=0.06

Figure S5. The SOM model generates topographic maps. Related to Figure 7. (A) Top row: position of center of receptive field for each postsynaptic cell. Bottom row: position of center of mass of synaptic connections. Left panel: at time 0, all synaptic weights are distributed equally, so that postsynaptic neurons response is not specific. Center panel: at time 100 postsynaptic responses and weights become more specific. Right panel: at time 12000 an ordered topographic map has emerged. (B) The model returns different final results after 12000 iterations. Top: the postsynaptic sheet develops the same orientation as the presynaptic sheet, as indicated by the location of the colored corners. Center: the map unfolds but with incorrect orientation, different from the retina. Bottom: The postsynaptic weights did not unfold properly (the retinotopic map is disrupted). Thus, the map develops overtime from a condition in which all cells are connected with almost equal weights, so that the position of all receptive fields is very close to the center, to a situation in which, after 12000 cycles of stimulation, the synaptic connections have been greatly refined and the receptive fields of each post-synaptic cells relocated to form an orderly topographic map. (C) Effect of molecular gradient and positional noise in the development of retinotopic maps. Initial maps for all combinations of $\sigma_{molecular} \in [0.1, 0.5, 1]$ and $\sigma_{noise} \in [0, 0.03, 0.06]$. The effect of the model parameters $\sigma_{molecular}$ and σ_{noise} is illustrated. A low value of dispersion in the molecular gradient and noise level gives an initial mesh very close to a perfectly deployed topographic map (upper left panel). Increasing the value of σ_{noise} (top to bottom in the figure) produces more disorganized initial maps. Increasing the value of $\sigma_{molecular}$ (left to right in the figure) produces less predetermined initial maps, with receptive fields for all cells very close to a uniform response, and the positions of the center of mass of the weights very close to the center.

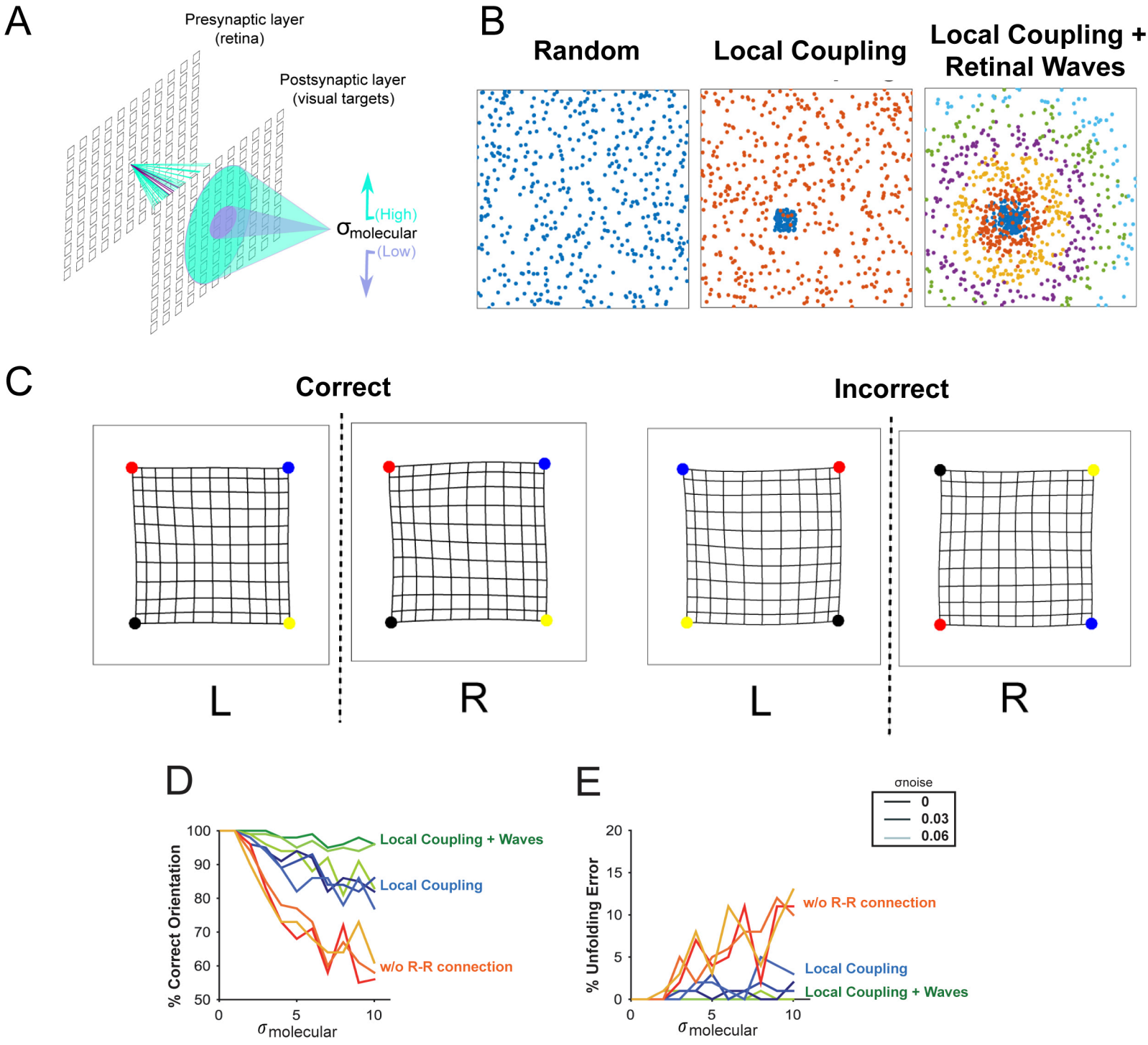
A
Presynaptic layer
(retina)
Postsynaptic layer
(visual targets)
(High)
σmolecular
(Low)
B
Random
Local Coupling
Local Coupling +
Retinal Waves
C
Correct
Incorrect
L
R
L
R
D
% Correct Orientation
100
90
80
70
60
50
0
5
10
σmolecular
Local Coupling + Waves
Local Coupling
w/o R-R connection
E
σnoise
0
0.03
0.06
% Unfolding Error
20
15
10
5
0
0
5
10
σmolecular
w/o R-R connection
Local Coupling
Local Coupling + Waves

Figure S6. Effect of molecular- and activity-dependent mechanisms on the development of bilaterally congruent topographic maps. Related to Figure 7.

(A) A gradient of different guidance molecules instructs initial targeting in the postsynaptic layer. To simulate the initial spread of the axons, the effect of the molecular gradient ($\sigma_{molecular}$) was modelled as a Gaussian function which increased the strength of the initial weights in the model based on the proximity of the presynaptic and postsynaptic neurons. Accordingly, high $\sigma_{molecular}$ values increased the initial spread of the axons, while low $\sigma_{molecular}$ values generated a lower initial coverage.

(B) Left panel: To model the absence of R-R connections, a set of completely random stimuli was applied. Center and right panels: The presence of R-R connections was modeled in two different ways: Local coupling - an initial region of stimulation (shown in blue) is followed by random activity. Local coupling + retinal waves - local coupling followed by a retinal wave traveling at a constant velocity.

(C) Retinotopic maps in mice have bilateral congruency, thus both topographic maps are arranged in the same orientation. By modelling the development of the right and left postsynaptic targets simultaneously, we were able to study the role of molecular guidance cues and synchronous activity in the development of bilateral congruency.

Examples of two simulations. Left: Correct bilateral congruency, i.e., left (L) and right (R) postsynaptic layers develop the same orientation as the presynaptic sheet as indicated by the order of the colored dots in the corners. Right: Incorrect bilateral congruency, in which, neither of the postsynaptic sheets coincides with the orientation of the retina nor coincide with each other as indicated by the order of colored dots.

(D) Percentage of maps with the correct orientation in both eyes (as a function of molecular gradients, $\sigma_{molecular}$), for the three types of stimuli (random stimulus that corresponds to no R-R connection (red), local coupling stimulus (blue) and local coupling plus retinal wave stimulus (green)). Noise levels are represented with different shades of the same color and correspond to σ_{noise}: 0, 0.03 and 0.06.

(E) Percentage of maps with topological defects or unfolding errors as a function of the molecular gradient for the three types of stimuli and the three different noise levels.

mRNA Unc5c

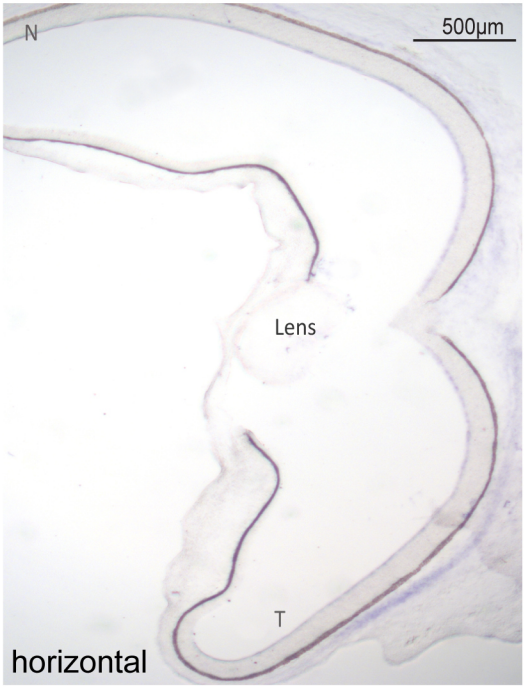

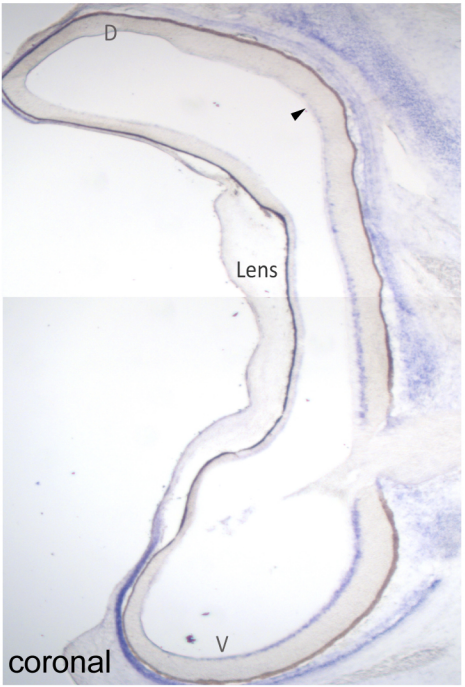

Figure S7. *Unc5c* expression in the developing chicken retina. Related to Figure 7.

Colorimetric ISH for *Unc5c* n horizontal and coronal sections of E7 chicken retinas. *Unc5c* is expressed in the RGC layer in a ventrocentral pattern similar to *Unc5c* expression in mouse and ferret. D, dorsal, N, nasal, T, temporal, V, ventral.

Parameter	Description	Value
λ	Weight decay term	0.1
τ	Time constant of λ decay	5555
ηt	Number of iterations	12000
σ_α	Lateral interaction influence	2
$\eta\eta$	Number of cells	11 x 11
σ_{noise}	Standard deviation (SD) of position noise	[0,0.21]
$\sigma_{molecular}$	SD of the molecular gradient	[0.1,10]

Table S1. Numerical values of model parameters. Related to Mathematical Model in STAR Methods and Figure S6.